



**HAL**  
open science

# On the Atomistic Origin of Internal Length Scale in Strain-Gradient Plasticity Models: the Case of Grain Boundary Structures and Energies

Houssam Kharouji, Vincent Taupin, Julien Guéno  

► **To cite this version:**

Houssam Kharouji, Vincent Taupin, Julien Gu  no  . On the Atomistic Origin of Internal Length Scale in Strain-Gradient Plasticity Models: the Case of Grain Boundary Structures and Energies. 2024. hal-04625373

**HAL Id: hal-04625373**

<https://hal.univ-lorraine.fr/hal-04625373v1>

Preprint submitted on 26 Jun 2024

**HAL** is a multi-disciplinary open access archive for the deposit and dissemination of scientific research documents, whether they are published or not. The documents may come from teaching and research institutions in France or abroad, or from public or private research centers.

L'archive ouverte pluridisciplinaire **HAL**, est destin  e au d  p  t et    la diffusion de documents scientifiques de niveau recherche, publi  s ou non,   manant des   tablissements d'enseignement et de recherche fran  ais ou   trangers, des laboratoires publics ou priv  s.



Distributed under a Creative Commons Attribution 4.0 International License

# On the Atomistic Origin of Internal Length Scale in Strain-Gradient Plasticity Models: the Case of Grain Boundary Structures and Energies

Houssam Kharouji<sup>a</sup>, Vincent Taupin<sup>a</sup>, Julien Guénoles<sup>a</sup>

<sup>a</sup>Université de Lorraine, CNRS, Arts et Métiers, LEM3, F-57070 Metz, France

---

## Abstract

The mechanical behavior of polycrystalline materials is controlled by microstructural size effects such as grain size or precipitate size. Various models of strain gradient plasticity have been proposed to capture such size effects, many of which have incorporated geometrically-necessary dislocation (GND) densities to introduce characteristic internal lengths. Recent developments have focused on models that incorporate a GND density into the internal energy functional. In such models, one needs to physically justify the functional form chosen and quantify the inherent internal length parameter. Our present study aims at probing relevant forms and internal length values in the case of grain boundary (GB) atomistic structures and core energies. We use an atomistic-to-continuum crossover approach that predicts an atomistic structure dependent GB energy by molecular static simulations, which is then recovered at the continuum-level by using a strain gradient, atomistically informed, field dislocation mechanics fast Fourier transform model. This allows (i) delineating the atomistic structure of GBs using an equivalent Nye GND density, and (ii) capturing the associated continuous elastic fields in the GB core area. We probe (i) a generalized non-quadratic GND density dependent energy functional to account for the core energy of defects, and (ii) elucidate the contributions of core versus elastic energy to the overall GB excess energy. We investigate and discuss the possible relevant choices for the energy functional form, as well as the physical origin of the inherent internal length parameter and its dependence to the types of grain boundaries, atomistic structures, and spatial resolution.

*Keywords:* strain gradient plasticity, internal length scale, grain boundary energy, Nye dislocation density, field dislocation mechanics, molecular statics, fast Fourier transform.

---

## 1. Introduction

The mechanical strength and plastic deformation behavior of polycrystalline materials are profoundly influenced by microstructural feature sizes, such as grains and precipitates. Grain boundaries, in particular, serve as primary contributors to the material's yield strength, impeding dislocation mobility by acting as barriers. The well-known example consisting of increasing the strength of polycrystalline metallic alloys by decreasing the grain size is called the Hall-Petch effect [1, 2]. Likewise, for a given volume fraction of precipitates, the flow stress increases with a decrease in the size of precipitate phase [3]. The influence of size effects on the mechanical hardening of certain architected materials, such as composites, is noteworthy. This connection is closely tied to channel slip mechanisms, like in nickel-based superalloys. Remarkably, channel slip exhibits a pronounced response to the geometry and width of channels, which directly affects strain hardening [4].

Modeling the size effects holds significant promise for materials engineering and design. Nonetheless, one important obstacle lies in correlating the observed size effects with an

internal length scale that is characteristic of the microstructures and mechanisms involved. For instance, the internal length scale may be the size of dislocation pile ups at grain boundaries, at hard particles or channel walls etc. Classical plasticity models often fail at predicting the size-dependent mechanical properties of materials, primarily because they lack such an internal length scale in the model formulation [5]. In the 1980s, Aifantis introduced a fundamental model of strain gradient plasticity to address this limitation. This model incorporates a back stress term as a function of the second gradient of the plastic slip, with a prefactor involving a single internal length scale parameter, to predict the width of shear bands [6, 7]. In their work, Fleck and Hutchinson suggest the necessity of incorporating more than a single internal length scale (three invariants of the plastic strain gradient tensor) into any phenomenological gradient plasticity theory, in order to accurately represent the effective plastic strain gradient. Other approaches within strain gradient plasticity framework were developed to account for size effects. Ashby [8] proposed a pioneering model suggesting the importance of considering Geometrically Necessary Dislocation (GND) densities to account for size effects. The model explains the Hall-Petch effect by considering grain size in the production rate of GND density that in turn induces alloy's work-hardening. In similar vein, a motivated strain gradient theory of plasticity based on lattice incompatibility was proposed by Acharya [9], in which

---

\*Corresponding author

Email address: julien.guenole@univ-lorraine.fr (Julien Guénoles)

gradient effects are incorporated in the hardening response. This incorporation introduces an intrinsic length-scale into the constitutive theory. Alternatively, Gurtin et al. developed a strain gradient single crystal plasticity model to account for internal length and size effects. In this thermodynamical approach, they demonstrate that the effects of energetic length scale impact the rate of kinematic hardening [10]. In the present work, our focus lies on models that incorporate the GND density into the internal energy functional, thus introducing an internal length as a supplementary material parameter [11–13].

Lately, several approaches proposed free energy potentials including the full dislocation density tensor as an argument within the framework of strain gradient plasticity [12]. Most applications utilizing strain gradient crystal plasticity (SGCP) theories rely on quadratic expressions of defect energy, which is added to the classical elastic energy. These serve as a bridge connecting free energy with dislocation densities and gradients of plastic slips [14–16]. Forest et al. [11] have inspected the relevant form of free energy functions of the dislocation density tensor in the context of strain gradient plasticity (SGP). They explored distinct free energy functions of the dislocation density tensor. Initially, they focused on examining the quadratic form extensively proposed in the literature. With such a choice, there is a prefactor consisting of a stiffness moduli (typically a shear modulus) multiplied by an internal length squared. The latter length is a model parameter. However, this approach was found to yield physically unrealistic scaling laws in the size-dependent response of laminate microstructures under shear [11]. As an alternative, they considered a rank-one defect energy, which exhibits linearity with respect to the norm of the dislocation density and yields better scaling laws. Motivated by the statistical dislocation theory of Groma [17], Forest et al. also incorporated the logarithm of the norm of the dislocation density tensor as a form of defect energy. Additionally, they introduced an alternative logarithmic potential based on the well-known Read–Shockley low angle grain boundary energy model [18]. In a related vein, Cai et al. [12] have recently introduced a generalized non-quadratic (power-law) defect energy formulation within a Gurtin-type strain gradient crystal plasticity framework. In this formulation, the defect energy is expressed as a function of dislocation norm raised to the power of  $n$ . An internal length to the power  $n$  is correspondingly introduced in the energy functional.

In the works mentioned above, the dislocation density energy term is usually referred to as a core energy term. In the present manuscript, we are interested in quantifying the internal length introduced in GND density core terms, and in possibly relating its value to a microstructural feature, thus making this internal length a physical parameter rather than an adjustable parameter. We consider atomic grain boundary structures and excess energies in this work. Recently, a novel method has been developed, combining atomistic simulations and continuum field dislocation mechanics (FDM), which aims at providing a continuum mechanics description of the

atomic structure of crystal defects such as dislocations and grain boundaries. Specifically, the model converts the atomic structure of defects into an equivalent Nye GND density. This approach satisfactorily captures the dislocation density associated with defects and their elastic fields by comparison with atomistic simulation results [19]. Hence, our model incorporates the continuous elastic fields and the elastic energy density linked to the distribution of a given GND density. The model further allows to integrate the dislocation density into a generalized non-quadratic (power law) energy functional, to evaluate its contribution to the total GB core energy. In this study, we concentrate on investigating and discussing the relevant energy functional forms, as well as the dependence of the associated internal length scale on grain boundary misorientation, structure, and spatial resolution, for various symmetrical tilt grain boundaries in copper. At first, we show that we can adjust the internal length parameter in the GND density energy term in order to retrieve reference GB energies predicted by classical molecular statics. We do so for GND density power exponent equal to one and two. We show that this length is very small and can be related to the defects composing grain boundaries. It is not a constant value and depends on the GBs considered. Finally, we investigate the dependence of this internal length on the simulation spatial resolution.

The structure of the paper is organized as follows: The section 2 details the procedure utilized to acquire the relaxed atomistic structure of symmetrical tilt grain boundaries (STGB). Section 3 provides an overview of the FDM approach, including the key equations. Following this, Section 4 delineates the methodology employed to derive the Nye GND density from atomic configurations for a given grain boundary, to be used as input in the FDM model simulations. In Section 5 and 6, and 7 we analyze the results, offer potential physical interpretations for the internal length and discuss the most appropriate choice for the core energy functional form.

## 2. Atomistic simulations of grain boundary: Structure and energy

All molecular statics simulations and calculations were performed using the Large-scale Atomic/Molecular Massively Parallel Simulator (LAMMPS) code [20]. An embedded atom method (EAM) potential for copper was employed to generate the relaxed atomic structures of  $[001]$  and  $[111]$  symmetrical tilt GBs [21]. This potential is fitted to accurately describe a variety of physical and mechanical properties of crystalline Cu, including stacking fault energy, grain boundary energies, and elastic moduli.

The GB are constructed within an  $x-y-z$  simulation box so that the GB plane normal is along the  $y$  direction, the tilt axis is along the  $z$  direction and the GB plane is contained within the  $x-z$  plane. To calculate the GB energies, we employed a bicrystal model with a given coincidence site lattice (CSL) matrix defined by the classical GB macroscopic degrees of freedom (DoF). To optimize the GB microscopic DoF, a large vari-

ety of GB configurations was obtained by applying rigid body translations of one grain with respect to the other in GB plane, as well as an atom deletion criterion to ensure that no atom have a neighbor closer than a cutoff distance  $r_c$ . In this work, we use a cutoff  $a_0 \frac{\sqrt{2}}{6} < r_c < a_0 \frac{\sqrt{2}}{2}$ , where  $a_0$  is the lattice parameter. Relaxation was conducted for each configuration using the conjugate gradient minimization algorithm, with a GB configuration considered optimized when the norm of the global force vector is below  $10^{-8}$  eV/Å. Finally, we select the lowest energy configuration. The GB energy is given by:

$$\Psi^{MS} = \frac{E - E_b}{2A}, \quad (1)$$

where  $E$  is the energy of the supercell containing the GB,  $E_b$  is the energy of a bulk supercell with the exact same number of atoms,  $A$  is the cross-section area on the  $x-z$  plane in the supercell. We divide over twice the surface area because each computational cell contains two opposing grain boundaries, owing to periodic boundary conditions. This procedure is largely employed in the literature [22, 19].

### 3. Continuum approach for grain boundary energy

The presence of dislocation distributions introduces elastic deformations within the crystal lattice, and induces a long-rang internal stress field [23]. In the following analysis, we introduce the concept of the field dislocation mechanics based on Nye dislocation density tensor, and the Kröner incompatibility equation [24] to describe the elastic fields of dislocation configurations. We assume the quadratic function form of the elastic strain energy density:

$$\Psi^{el} = \frac{1}{2} \boldsymbol{\varepsilon}^e : \mathbf{C} : \boldsymbol{\varepsilon}^e, \quad (2)$$

where,  $\boldsymbol{\varepsilon}^e$  denotes the elastic strain tensor, and  $\mathbf{C}$  is the tensor of elastic moduli. In linear elasticity framework, the elastic strain energy density is given as a function of the components of the Cauchy stress tensor  $\boldsymbol{\sigma}$  by:

$$\Psi^{el} = \frac{1}{2} \sigma_{ij} \varepsilon_{ij}^e. \quad (3)$$

To calculate the elastic strain induced by a given dislocation distribution, we need to calculate first, the elastic distortion. In the absence of dislocation, this tensor is a curl-free compatible gradient tensor, and it is defined as the gradient of the elastic displacement. Nonetheless, in the presence of dislocations, integrating the elastic distortion along a Burgers circuit  $C$ , delimitating a surface  $S$  threaded by dislocation lines, results in an elastic displacement jump between the final and starting points, which corresponds to the net Burgers vector  $\mathbf{b}$  of the dislocation lines. This is represented by the following equation:

$$\mathbf{b} = \int_C \mathbf{U}_e d\mathbf{x}, \quad (4)$$

where  $\mathbf{x}$  denotes the position vector. Applying Stokes' theorem to the above equation gives:

$$\mathbf{b} = \iint_S \mathbf{curl}(\mathbf{U}_e) \cdot \mathbf{n} dS. \quad (5)$$

The total Burgers vector of all dislocation lines crossing the surface  $S$  with normal  $\mathbf{n}$  and bounded by the curve  $C$  can be geometrically described through a second-order tensor known as the dislocation density tensor or so-called Nye tensor:

$$\mathbf{b} = \iint_S \boldsymbol{\alpha} \cdot \mathbf{n} dS. \quad (6)$$

Through the identification in both above integral equations, the Nye tensor can be expressed as a function of the **curl** of the elastic distortion, as follows:

$$\boldsymbol{\alpha} = \mathbf{curl}(\mathbf{U}_e) \quad (7)$$

The equation (7) establishes a link between the Nye tensor and the incompatibility of elastic distortion. When the Nye density distribution is null, the elastic distortion tensor becomes a gradient compatible tensor (with a zero **curl**). In this equation, the curl operator extracts the incompatible part of the elastic distortion, which is not a gradient compatible tensor. This results in a discontinuity in elastic displacement when integrated along the Burgers circuit. In this context, we apply the Stokes Helmholtz decomposition proposed by Acharya [25] to decompose the elastic distortion into a compatible, curl-free part  $\mathbf{U}_e^{\parallel}$ , which is a gradient tensor, and an incompatible part which is a non-gradient tensor, **curl** part  $\mathbf{U}_e^{\perp}$ :

$$\mathbf{U}_e = \mathbf{curl}\boldsymbol{\chi} + \mathbf{grad}\mathbf{w} = \mathbf{U}_e^{\perp} + \mathbf{U}_e^{\parallel}. \quad (8)$$

Applying the **curl** operator to equation (8) allows for the reformulation of equation (7), yielding Kröner's incompatible equation of distortion within small strain framework [24].

$$\boldsymbol{\alpha} = \mathbf{curl}(\mathbf{U}_e^{\perp}) \quad (9)$$

Ultimately, the incompatible part, solution to equation (9), should not incorporate compatible part and must therefore be purely rotational. From the Stokes-Helmholtz decomposition, incompatible part of the elastic distortion must satisfy  $\mathbf{div}(\mathbf{U}_e^{\perp}) = \mathbf{0}$ . By applying the **curl** operator to equation (9), utilizing the identity  $\mathbf{curl}(\mathbf{curl} \mathbf{A}) = \mathbf{grad}(\mathbf{div} \mathbf{A}) - \mathbf{div}(\mathbf{grad} \mathbf{A})$ , the incompatible elastic distortion must be a solution to the following Poisson-type equation:

$$\mathbf{div}(\mathbf{grad}\mathbf{U}_e^{\perp}) = \Delta\mathbf{U}_e^{\perp} = -\mathbf{curl}(\boldsymbol{\alpha}). \quad (10)$$

This equation can be solved through spectral numerical techniques, employing Fast Fourier Transform (FFT) algorithms tailored for computing internal stress fields linked with dislocation density distributions in both elastically homogeneous [26], and in heterogeneous materials [27]. Once the incompatible elastic distortion is determined, the next step thus, is to determine the compatible part in order to obtain the total elastic distortion. Subsequently, the mechanical equilibrium equation is

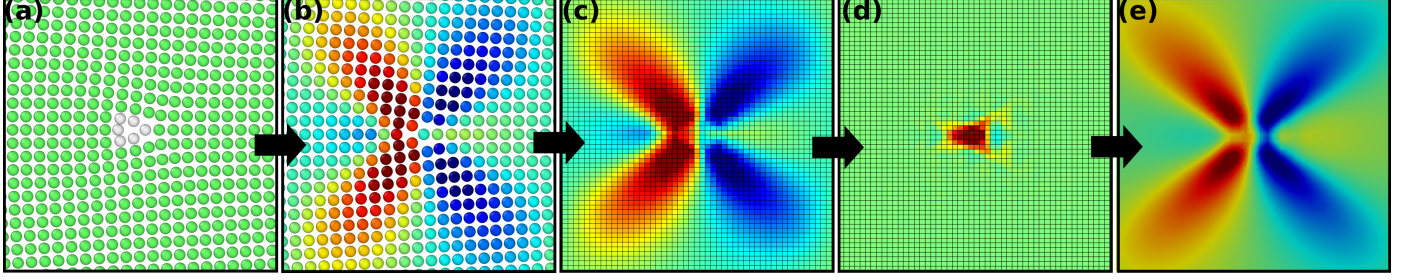


Figure 1: Schematic illustration of the atomistic to continuum transfer method. (a) 2D visualization of the atomic structure of an isolated structural unit composing a [00 1] symmetrical tilt GB in copper. Atoms are colored according to CNA, Green atoms: FCC structure; white atoms, undefined environment. (b) Visualization of the per-atom lattice correspondence tensor (component  $G_{12}$ ) obtained by Hartley & Mishin algorithm. (c) Interpolation of  $G_{12}$  onto a regular FFT grid, with a resolution of 0.5 Å. (d) Calculation of the component  $\alpha_{23}$  of the Nye tensor onto the FFT grid. (e) 2D map of elastic distortion obtained after solving the FDM equations, which can be compared to (b).

solved. In the presence of dislocations and without considering inertia effects, it is expressed as follows:

$$\mathbf{div}(\boldsymbol{\sigma}) = \mathbf{div}(\mathbf{C}:\mathbf{U}_e) = \mathbf{div}(\mathbf{C} : (\mathbf{U}_e^\perp + \mathbf{U}_e^\parallel)) = 0. \quad (11)$$

Using the definition of the compatible elastic distortion  $\mathbf{U}_e^\parallel$  (equation (8)), and defining the vector  $\mathbf{f}^\perp = \mathbf{div}(\mathbf{C}:\mathbf{U}_e^\perp)$  as a volumetric force resulting from the elastic incompatibility associated with dislocations, we rewrite this equation as:

$$\mathbf{div}(\mathbf{C} : \mathbf{grad} \mathbf{w}) + \mathbf{f}^\perp = \mathbf{0}. \quad (12)$$

where the unknown is the elastic displacement field  $\mathbf{w}$ . Similarly, we solve the above equation using an FFT spectral solver [27]. We notice that the components of the elastic moduli tensor  $\mathbf{C}$ , are calculated using molecular statics simulations. They are in good agreement with experimental data [21]. After determining  $\mathbf{w}$ , we can compute the corresponding compatible distortion, enabling us to identify the total elastic distortion and subsequently assess the stress tensor. Once the elastic fields are obtained, the elastic strain energy is calculated. In this work, we adopt the classical decomposition of the free energy  $\psi$  into an elastic strain energy  $\psi^{el}$  and a defect energy  $\psi^c$ . Building on the work of Jebahi *et al.* [12] we propose a generalized power-law defect energy formulation within Gurtin-type strain gradient crystal plasticity model. Thus, the total free energy is given by the following equation:

$$\psi = \psi^{el} + \psi^c = \frac{1}{2} \boldsymbol{\varepsilon}^e : \mathbf{C} : \boldsymbol{\varepsilon}^e + \frac{1}{n} \mu \ell^n \|\boldsymbol{\alpha}\|^n \quad (13)$$

Here,  $\mu$  and  $\ell$  represent the shear modulus and an energetic characteristic internal length scale, respectively.  $\|\boldsymbol{\alpha}\|$  denotes the norm of the Nye density tensor, while  $n$  is an integer that will take either the value 1 or 2 in the following. The parameter  $\ell$  is the internal length on which we focus in the present work. In the following, we aim at quantifying its value, its dependence on the atomic structures of grain boundaries and on the spatial resolution, i.e., on the scale at which we look at grain boundaries in terms of dislocation densities.

#### 4. Atomistic to continuum approach

In this section, we provide a brief summary of the so-called G method used to extract a dislocation density from the atomic structure of grain boundaries. Our earlier study [19] shows details on this approach that was applied to various defects. Essentially, the method relies on deriving the per-atom lattice correspondence tensor using the original algorithm developed by Hartley & Mishin [28, 29]. This tensor is defined as the transpose of the inverse elastic transformation tensor and is computed by comparing the local environment surrounding each atom in a dislocated (current) configuration to the corresponding local environment around the same atom in a bulk (reference) configuration (Fig. 1(b)). Relevant components of the  $\mathbf{G}$  tensor are interpolated onto regular FFT grid where FDM calculations will be run, as illustrated in Fig 1(c). On this grid, we employ a centered finite difference scheme to compute the **curl** of the  $\mathbf{G}$  tensor, yielding the Nye dislocation density tensor  $\boldsymbol{\alpha}$  (Fig. 1(d)). The latter is used as input to solve the FDM equations, leading to the continuous elastic distortion field (Fig 1(e)), which can be compared to the one obtained by the Hartley and Mishin algorithm. The method was successfully applied to dislocations, low angle and high angle GBs, and interactions between dislocations and high/low-angle grain boundaries [19]. It was also concluded that this method is better than directly interpolating the per-atom Nye tensor evaluated using the Hartley and Mishin algorithm.

Since the FDM field equations are numerically approximated on a regular FFT grid, we assessed different interpolations of atomistic data onto the FFT grid. We analyze the effect of the grid mesh size and then compare the results with atomistic data in terms of Nye density and elastic strain fields. Fig. 2 illustrates the influence of FFT grid resolution on Nye dislocation density distributions of an isolated structural unit in the low angle grain boundary in copper ( $\Sigma 401(20\bar{1}0)[001]$ ), with  $5.72^\circ$  misorientation angle. As depicted in the Fig. 2(b), the transfer method successfully captures the details of the edge dislocation density at the finest resolution examined (0.5 Å), but demonstrates a spread-out in the dislocation density distribution for resolutions exceeding 2 Å (Figs. 2(d), and 2(e)). For a fine resolution, we will explicitly capture and model all

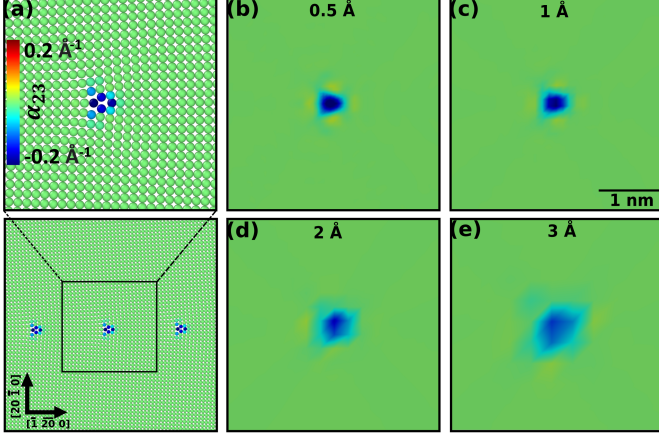


Figure 2:  $\Sigma 401(20\bar{1}0)[001]$   $5.72^\circ$  low angle grain boundary in copper. Effect of FFT grid resolution on Nye density distributions  $\alpha_{23}$ . (a) Per-atom component  $\alpha_{23}$  of the Nye tensor obtained using the Hartley-Mishin algorithm. (b), (c), and (d) 2D maps of the edge dislocation density using the transfer method, with FFT grid resolutions of 0.5 Å, 1 Å, 2 Å, and 3 Å respectively.

defects composing the GBs. We expect to accurately describe the elastic fields, as shown below. However, when increasing the resolution, we progressively miss the description of defects composing the GBs. We will progressively miss the description of elastic fields at the GBs, and the description of GBs will tend to a continuous density of dislocation density along the interfaces. The latter density corresponds to the elastic curvature at GBs, as would be obtained from EBSD orientation maps.

We indeed evaluated the effect of the FFT grid resolution on the distribution of the in-plane shear component  $\varepsilon_{12}$  of the elastic strain field for the isolated structural unit in the LAGB. Fig. 3 illustrates comparison between the distribution of continuous strain fields acquired through the transfer method and atomic strain fields, across various FFT grid resolutions. The results demonstrate accurate representation of elastic strain at dislocation cores with finer resolutions. A prior quantitative comparison rigorously examined the profiles of elastic strain fields in comparison to atomistic strain, revealing that the transfer method effectively captures elastic fields away from defect cores even at resolutions of 2 Å or higher. The approach demonstrates efficiency not just in elastic strain, but also in producing significant stress field distributions, which are consistent with the virial stress derived from molecular statics simulations [19].

## 5. Quantification of the internal length

By matching the GB excess energy predicted by FDM to that measured by molecular statics for all GBs modeled, we can quantify the characteristic internal length introduced in defect energy functional in equation (13). We initially assume that the grain boundary free energy predicted by FDM can be equal to the GB energy obtained from molecular statics simulations.

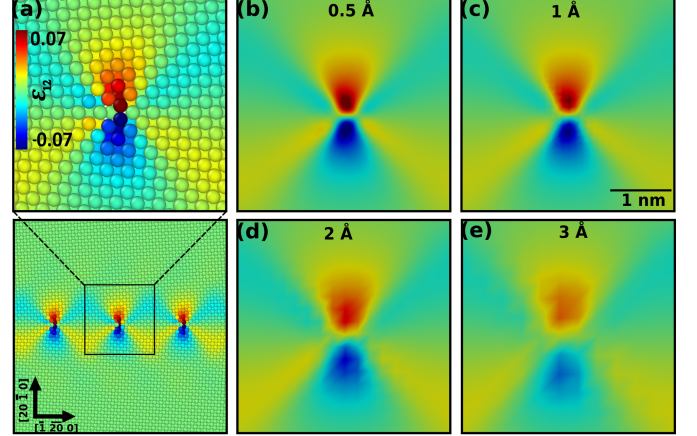


Figure 3:  $\Sigma 401(20\bar{1}0)[001]$   $5.72^\circ$  low angle grain boundary in copper. Effect of FFT grid resolution on elastic shear strain field distribution. (a) Visualization of the per-atom component  $\varepsilon_{12}$  of the elastic strain tensor obtained using the Hartley & Mishin algorithm. (b), (c), and (d) 2D maps of the shear elastic strain obtained using the transfer method, with FFT grid resolutions of 0.5 Å, 1 Å, 2 Å, and 3 Å respectively.

This is indeed the case in the following. For a given GB, we have access to the Nye tensor and the elastic fields in the FDM simulation results. We have an elastic energy density value at any point  $r$  in the domain  $V$  as well as a local core energy. It is thus possible to integrate these two energies over the simulation volume  $V$ , divide it by twice the area of GBs, in order to have the excess energy of GBs. This reads:

$$\Psi^{MS} = \Psi^{el} + \Psi^c = \frac{1}{2A} \left( \iiint_V \Psi^{el}(r) dV + \frac{1}{n} \mu \ell^n \iiint_V \|\alpha\|^n dV \right), \quad (14)$$

where  $A$  is the GB area. The only adjustable parameter in the above equation, to match the FDM GB excess energy to that of molecular statics, is the internal length  $\ell$ . From the above equation, the characteristic internal length can indeed be quantified from:

$$\ell = \left( \frac{n}{\mu} (\Psi^{MS} - \Psi^{el}) \frac{2A}{\iiint_V \|\alpha\|^n dV} \right)^{\frac{1}{n}}. \quad (15)$$

This equation can be used for every GB studied in the following. It can be used to assess the dependence of  $\ell$  on GB atomic structure, dependence on the exponent  $n$  (1 or 2) in the core energy functional, and on spatial resolution in FDM simulations.

## 6. Results

The modeling strategy presented above is now applied to various symmetrical tilt grain boundaries in copper with  $[001]$  and  $[111]$  rotation axes. The results for the  $[001]$  STGB are shown in Figure 4, with an FFT resolution grid size of 0.5 Å.

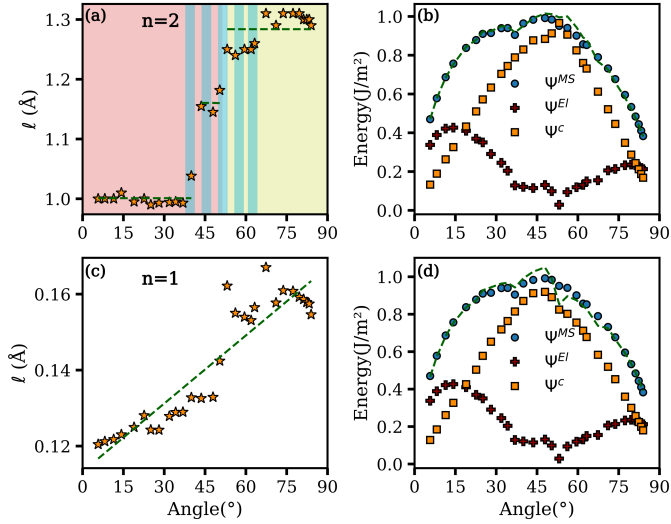


Figure 4: Characteristic internal length  $\ell$  and energies as a function of misorientation angle for  $[001]$  symmetrical tilt grain boundaries (GB) in copper. (a) and (c) shows ideal  $\ell$  obtained by fitting GB energies from FDM to those derived from molecular static simulations for  $n = 2$  and  $n = 1$ , respectively. Dashed lines represent trends discussed in the text. (b) and (d) shows several GB energies: Elastic Strain Energy  $\Psi^{El}$ , Core Energy  $\Psi^C$ , and energy from molecular static simulations  $\Psi^{MS}$ . Dashed curves indicate the sum of elastic and core energy. The Core Energies  $\Psi^C$  from (b) and (d) are obtained via FDM with the  $\ell$  values given by the dashed lines in (a) and (c). The FFT grid resolution is  $0.5 \text{ \AA}$ . The background colors in (a) indicate the structural units forming the GB, as shown in Fig. 6: red, blue, yellow for B, C and D structural units type.

For this rotation axis, the misorientation angle ranges from  $0^\circ$  to  $90^\circ$ , thus including both low and high angle GBs. To ensure periodic boundary conditions, all GBs investigated here are coincidence site lattice (CSL) boundaries [30]. Fig. 4(a), and Fig. 4(c) depict the optimal "ideal" internal length  $\ell$  as obtained from equation (15). Figure 4(a) focuses on  $\ell$  obtained using quadratic defect energy ( $n = 2$ ). One can identify 3 different regimes for the evolution of the internal length as a function of the misorientation angle. The first regime lies in between  $0^\circ$  and  $36.87^\circ$ , where  $\ell$  maintains a quasi-steady value of approximately  $1 \text{ \AA}$ . Note that the limit of this regime corresponds to the  $\Sigma 5(310)$  GB. The subsequent regime comprises GBs between  $36.87^\circ$  and  $53.13^\circ$ , where the internal length is increased. Finally, the third regime concerns angles ranging from  $53.13^\circ$  to  $83.97^\circ$ , where the internal length tends to saturate with a constant value close to  $1.3 \text{ \AA}$ . We add trends for these regimes with horizontal dashed lines in the figure. Fig. 4(b) now illustrates the relationship between grain boundary energy and misorientation angle, as determined by molecular statics simulations (circle symbols) and FDM (dashed curve), still for  $n = 2$ . Importantly, it shows the split of the grain boundary energy into elastic strain and core energy in the FDM simulations, with square and cross symbols, respectively. Based on the three regimes of the characteristic "ideal" internal length profile, we chose  $\ell$  as the average of the "ideal"  $\ell$  within the corresponding misorientation range. This averaged  $\ell$  is used to calculate  $\Psi^C$ . The idea is to see what FDM simulations can predict in terms of core energies  $\Psi^C$

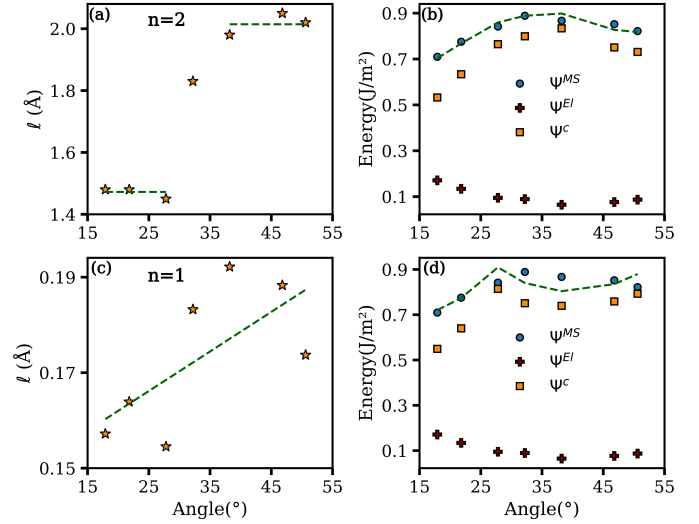


Figure 5: Characteristic internal length and grain boundary energies as a function of misorientation angle for  $[111]$  symmetrical tilt grain boundaries in copper. The FFT grid resolution is  $0.5 \text{ \AA}$ . (a), and (c) Ideal internal length to align overall grain boundary energies obtained via FDM with those derived from molecular static simulations for  $n = 2$  and  $n = 1$ , respectively. Dashed lines represents trends discussed in the text. (b) and (d) Grain Boundary Energies: Elastic Strain Energy  $\Psi^{El}$ , Core Energy  $\Psi^C$  obtained via FDM for various  $\ell$  values (indicated by dashed lines), and energy from molecular static simulations  $\Psi^{MS}$ . Dashed curves indicate the sum of elastic and core energy.

when using a fixed  $\ell$  value (dashed lines in Fig. 4(a)), instead of using the ideal fitted value for each GB (star symbols in Fig. 4(a)). Note that the elastic energy  $\Psi^{El}$  does not change whatever the choice of the internal length as it is an output of the FDM simulations. In this context, we observe a satisfactory agreement between the continuum and the atomistic models, as shown in Fig. 4(b) by the large overlap of the total GB energy predicted by molecular statics (circle symbols) and by FDM (dashed curve). The order of magnitude of the internal length and its evolution into three regimes in relation with atomic structures of GBs is discussed in section 7.1. Figure 4(b) indicates that, as the misorientation increases, there is a corresponding increase in the relative contribution of the core energy, displaying two peaks for the  $\Sigma 5(310)$  and  $\Sigma 5(210)$  boundaries at misorientations of  $36.9^\circ$  and  $53.1^\circ$ , respectively. Conversely, the elastic strain energy exhibits cusps for the same boundaries. These cusps reflect the self-screening effect of elastic fields within the GB, occurring when the separation distance between structural units diminishes and becomes small. Van Beers et al. [31] have noted similar behavior, by using the Frank-Bilby [32] and Read-Shockley [18] models to predict the GB excess energy through molecular statics simulations. We provide a more detailed comparison of FDM results with the model by Van Beers in section 7.2. Now considering a core power exponent  $n = 1$ , it is observed that a linear fit (Fig. 4(c)) of the internal length provides the most accurate approximation for the GB energies. This defines one unique regime for the internal length within the complete misorientation range. As opposed to what we observed for  $n = 2$ , the averaged  $\ell$  used in the calculation of  $\Psi^C$  is not constant but linearly proportional

to the misorientation angle. The GB energies calculated using FDM exhibit excellent agreement with atomistic GB energies, particularly for low-angle GB (Fig. 4(d)). The evolution of elastic and core energies components is similar for the two values of the core power exponent.

A similar analysis is now conducted on seven  $[111]$  symmetrical tilt grain boundaries in copper, as depicted in Figure 5. For this particular misorientation axis, it is sufficient to consider the misorientation angle in the range from  $0^\circ$  to  $60^\circ$ . Figure 5 presents the comparative results for both values of the core energy power exponent  $n$ . The misorientation dependence of  $\ell$  for  $n = 2$  is illustrated in Fig. 5(a). The "ideal"  $\ell$  values were again determined through a fitting of equation (15) to the atomistic results. We identify two distinct regimes: the first one includes the low-angle grain boundaries, while the second one spans the range from  $38.2^\circ$  to  $50.6^\circ$ . As above, we calculate by FDM the GB energy by averaging the internal length value across each regime. The resulting energy versus misorientation is depicted by the dashed curve in Figure 5b and reveals a good agreement with atomistic results (circle symbols). Note that due to the limited number of CSL grain boundaries for this particular GB misorientation axis, the choice of averaged  $\ell$  remains quite arbitrary. This is even more pronounced for  $n = 1$  (Fig. 5(c)), where we opted for a linear fit. The energetic dependence to misorientation is shown in Fig. 5(d). Similar to the analyses outlined above for  $n = 2$ , the elastic energy diminishes until it reaches a minimum value for the CSL GB of highest symmetry, that is the  $\Sigma 7 (123)$  GB of misorientation  $38.2^\circ$ . This decrease can again be attributed to the screening effect of the elastic fields. Regarding the core energy, it follows a non-linear evolution with misorientation.

## 7. Discussion

### 7.1. Relation between internal length and GB structure

The GB structure can be described using the structural unit model (SUM) [34, 35], as shown in figure. 6 for the  $[001]$  STGB. A correlation emerges between the behavior of the characteristic internal length and the structural units (SU) constituting the grain boundaries, for  $n = 2$ . Let us consider the first regime of the  $[001]$  GB that covers angles ranging from  $0^\circ$  to  $36.87^\circ$ . Each of these GB is formed by B SU and consists of topologically identical kite-shaped units, differing only in the distance between them (figure. 6(a)). For the low-angle grain boundaries within this regime, the GB structure can be represented as an array of edge dislocations with cores formed by the B kite-shape SU, and a Burgers vectors  $\mathbf{b} = a[010]$ , with  $a$  the lattice parameter. Using the same interatomic potential for copper, Cahn et al. [36] have reported the same GB structure. The STGB within the second regime ( $36.87^\circ$  to  $53.13^\circ$ ) are formed by B and C SU, as illustrated by Figure 6(b) with the  $\Sigma 29(520)43.6^\circ$  that consist of  $|BC|$  SU. The last regime (from  $53.13^\circ$  to  $90.00^\circ$ ) can be decomposed in two sub parts.

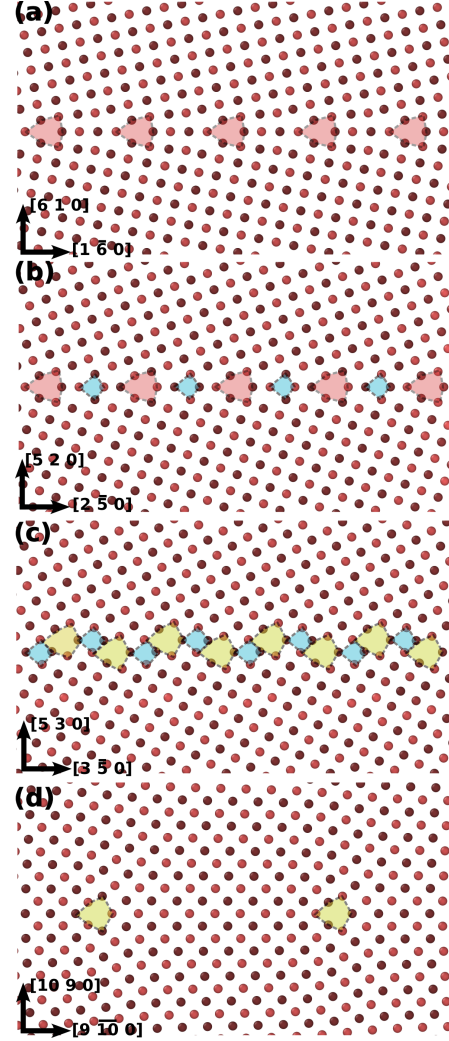


Figure 6: Optimized structure of  $[001]$  symmetrical tilt grain boundaries in copper at 0 K, visualized using OVITO [33]. (a)  $\Sigma 37 (610) 18.92^\circ$ , (b)  $\Sigma 29 (520) 43.603^\circ$ , (c)  $\Sigma 37 (530) 61.93^\circ$  and (d)  $\Sigma 181 (1090) 83.974^\circ$ . The structural units are highlighted by dashed line and colored area: red, blue and yellow for the structural units of type B, C and D, respectively. Atoms on adjacent parallel  $\{001\}$  planes are represented with different shades of red.

The first one consist on combinations of C and D SU (Fig. 6(c) with a  $\Sigma 37 (530) 61.93^\circ$ ) whearease the second one consits on D SU only (Fig. 6(d) with a  $\Sigma 181 (1090) 83.974^\circ$ ). Specifically, this very last regime corresponds to low-angle grain boundaries described by dislocation arrays of  $\mathbf{b} = -a/2[110]$  with C kite-shape SU. The relationship between SU and misorientation angles for all these 4 regimes is summarized on Fig. 4(a).

### 7.2. Comparison with Van Beers model

In this work, we compare our FDM results with a model proposed by Van Beers et al. [31, 37, 38], where atomistic simulations are employed to derive GB energies and extract their structural characteristics. These features are subsequently incorporated into the Frank-Bilby equation to calculate the GB



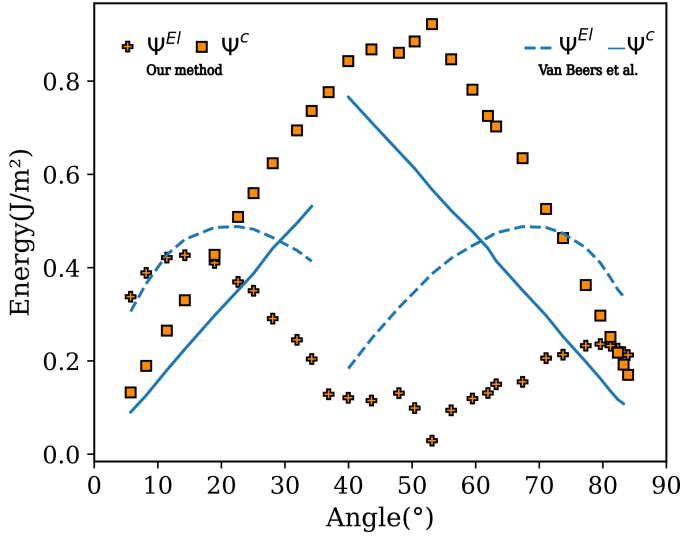


Figure 7: Comparison of elastic and core energies for [001] symmetric tilt boundaries in copper, as a function of misorientation. Orange squares, and filled crosses: core and elastic energy derived from our study, respectively; Solid/dashed blue lines: core and elastic energy extracted from the work of Van Beers et al., respectively.

dislocation content to finally describe the GB core and elastic energy based on the Read and Shockley model. The elastic strain energy, screening included, as a function of the misorientation angle is represented using a logarithmic relationship based on the Read-Shockley formulation. The comparison between our model and that of Van Beers et al. reveals similar features (figure 7). From a general standpoint, it appears that Van Beer’s model tends to overestimate elastic energy and underestimate core energy. In our model, the elastic energy is lower and shows more fluctuations. As a lower elastic energy implies a stronger core energy, the lower energy of our model comes from explicitly modeling the structural units. While Van Beer’s model determines this energy through fitting to the total energy obtained atomistically, our approach relies on a purely mechanical transfer method to calculate the elastic strain energy.

We observe similarities in the general trend of both models, particularly regarding the dependence of core and elastic energies on GB misorientation angle. Van Beer’s model computes core and elastic energies based on a reference structure in which the dislocation content is defined. It considers two modes of dislocations Burgers vector relative to  $\Sigma 5(3\ 1\ 0)$  misorientation angle: one branch with a Burgers vector of [001] for GB between  $[5.725^\circ, 36.87^\circ]$ , and a second branch for boundaries between  $[36.87^\circ, 83.974^\circ]$ . However, this differentiation fails to account for the screening effect of elastic fields for GB with high misorientation, characterized by either by very short periods of SU or composed of mixed SU. This effect is notably observed between the  $\Sigma 5(3\ 1\ 0)$  and  $\Sigma 5(2\ 1\ 0)$  GB: the predictions of Van Beer’s model diverge largely from the predictions of our approach, where cores are simulated using a Nye distribution.

### 7.3. Effect of the FFT grid resolution on the internal length

Figure 8 illustrates the effect of the FFT grid resolution on the internal characteristic length  $l$ . A strong dependency of  $l$  on the resolution is observed. Across resolutions ranging from 0.5 Å to 2 Å,  $l$  exhibits various regimes with significant changes for both  $n = 1$  and  $n = 2$  (Figs. 8(a) and 8(d)). It is notable that higher values of  $l$  are associated with low angle grain boundaries. At higher resolutions, the behavior of  $l$  as a function of GB misorientation angle becomes parabolic for  $n = 2$  (Fig. 8(c)) and assumes a "v" shape for  $n = 1$ , with a minimum around  $45^\circ$  (Fig. 8(f)). In particular, starting from a resolution of 7 Å onward, the curves of the characteristic length tend to be similar, especially for the case  $n = 1$ . Figures 8(g)-(i) and 8(j)-(l) depict the effect of resolution on elastic energy and core energy. It is observed that for finer resolutions, the behavior of elastic energy  $\Psi^{El}$  with misorientation displays a consistent trend. However, as spatial resolution increases, the elastic energy decreases. Particularly, at high resolutions up to 7 Å, the elastic energy tends towards zero, suggesting an equivalence between grain boundary excess energy and core energy. As aforementioned, the increase in spatial resolution results in a less accurate representation of structural units in terms of dislocation density, which ultimately results in the loss of elastic fields nearby dislocation cores. We remind that Figure 3 demonstrates the impact of FFT resolution on the distribution of the Nye density and elastic fields.

We now aim to analyze the evolution of the internal length  $l$  at much higher resolutions (up to the micronmeter), which is the typical resolution used for modeling polycrystals and GBs in strain gradient plasticity models. Our results indicate that, while we may not fully capture elastic energy for large resolutions, we can still approximate GB energy by considering the core energy term. Reasonably assuming negligible elastic strain fields for large resolutions, the Nye tensor reduces to lattice or elastic curvatures. When observing a grain boundary at the micron scale, we essentially observe a band of constant dislocation density along the boundary, which indeed corresponds to an elastic curvature along the GB. This is exactly what is observed when deriving GB Nye dislocation density from Electron Backscatter Diffraction (EBSD) orientation maps. By neglecting elastic strains, certain components of the curvature tensor can indeed be accessed experimentally from the elastic rotations measured by EBSD. This suggests the possibility of estimating the GB energy as a function of curvature.

For this purpose, we explicitly establish an analytical relationship between the characteristic internal length " $l$ " and the FFT resolution " $\Delta x$ ". This will be achieved by deriving the Nye tensor from elastic curvatures. Starting from the Field dislocation mechanics, the distortion  $\mathbf{U}$ , in a small deformation setting, comprises symmetric part (strain tensor  $\boldsymbol{\varepsilon}$ ) and a skew-symmetric part represented by the rotation tensor  $\boldsymbol{\omega}$ . The corresponding rotation vector is denoted as  $\vec{\omega}$ . The elastic curvature tensor  $\boldsymbol{\kappa}_e$  is defined by [39]:

$$\boldsymbol{\kappa}_e = \mathbf{grad}\vec{\omega} = \mathbf{curl}\mathbf{l} + \mathbf{K} = \mathbf{grad}\vec{\omega} + \boldsymbol{\varepsilon}^e + \frac{1}{2}tr(\boldsymbol{\alpha})\mathbf{I} - \boldsymbol{\alpha}^t, \quad (16)$$

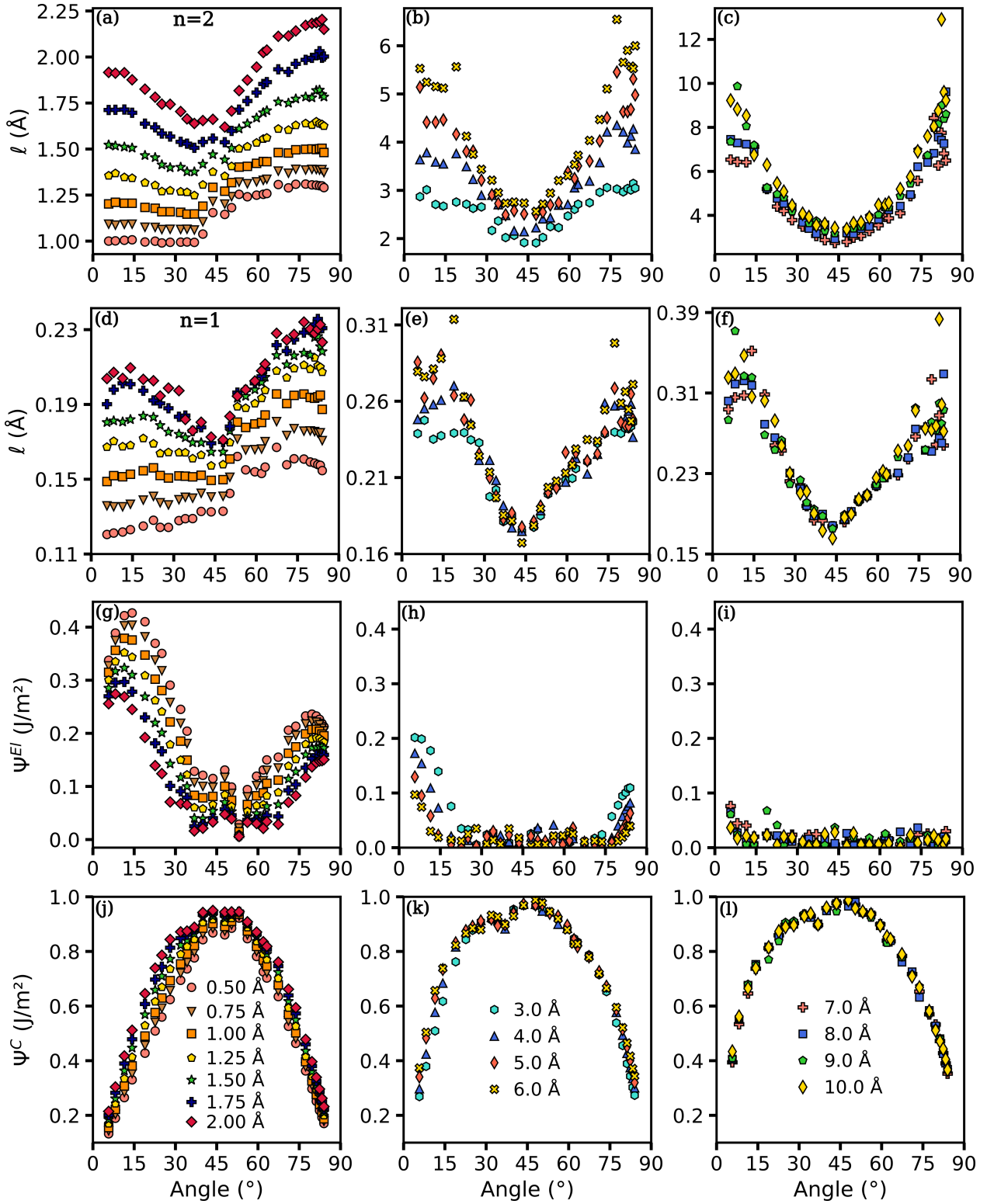


Figure 8: Effect of FFT grid resolution on the internal characteristic length, core and elastic energies as a function of misorientation angle for [001] symmetric tilt grain boundaries in copper. (a)-(c) Internal length for  $n = 2$ . (d)-(f) Internal length, for  $n = 1$ . (g)-(i) GB elastic energy. (j)-(l) GB core energy.

where  $\mathbf{K}$  is the Nye curvature and  $\mathbf{I}$  is the identity tensor. Above, we have shown that at high resolutions, elastic energy reaches low values ( $\varepsilon^e \rightarrow 0$ ), and the core energy's contribution to the total GB energy is dominant. Since only edge dislocation densities are present in the studied tilt GBs, this enables us to rewrite the equation 16 as:

$$\boldsymbol{\kappa}_e = \mathbf{grad}\vec{\omega} = -\boldsymbol{\alpha}^t. \quad (17)$$

As a consequence, the norm of the Nye tensor can be approximated as:

$$\|\boldsymbol{\kappa}_e\| = \|\mathbf{grad}\vec{\omega}\| = \frac{\Delta\theta}{\Delta x} = \|\boldsymbol{\alpha}^t\|, \quad (18)$$

where  $\Delta\theta$  is the GB misorientation and  $\Delta x$  is the FFT resolution. The norm of the Nye tensor is basically the misorientation jump between two points across the GB separated by a distance  $\Delta x$ . In the absence of elastic strains, the GB energy becomes:

$$\Psi^{MS} = \Psi^c = \frac{1}{A} \left( \frac{1}{n} \mu \ell^n \iint \|\boldsymbol{\alpha}\|^n dV \right), \quad (19)$$

which allows to establish the following internal length analytic equation:

$$\ell = \left( \frac{n\Psi^{MS}}{\mu\Delta\theta^n} \Delta x^{n-1} \right)^{\frac{1}{n}} \quad (20)$$

Figure 9 depicts the behavior of the average characteristic internal length as a function of the spatial resolution on a log-log plot. This analysis reveals distinct behaviors depending on the value of power law exponent  $n$ . For  $n = 1$ , minimal oscillations in " $\ell$ " are observed at lower resolutions. However, beyond a resolution of 7 Å, the variation of " $\ell$ " stabilizes and our transfer method aligns with the analytic model. This stabilization indicates that the characteristic internal length becomes independent of the spatial resolution (as implied by equation 20) and suggests that  $n = 1$  might be a relevant choice for modeling the grain boundaries as curvatures at higher scales. In contrast, the behavior for  $n = 2$  is different. As the resolution increases, the average  $\ell$  also increases until reaching the 7 Å threshold. Beyond this resolution,  $\ell$  exhibits a linear variation (in log scale) also implied by equation 20. This linear trend suggests that for  $n = 2$ , the internal length remains resolution-dependent, increasing with spatial resolution. Interestingly, at resolutions on the order of the micron, the internal length approaches towards values commonly utilized in strain gradient plasticity modeling of grain boundaries [40].

#### 7.4. On the choice of power exponent $n$ and internal length scale $\ell$

When modeling size effects occurring during elastic and/or plastic deformation, strain gradient approaches introducing an additional strain gradient based free energy term can be used. In addition to the form of this additional free energy functional, a characteristic internal length parameter  $\ell$  is introduced and needs to be calibrated to properly retrieve size effects, scaling laws or elastic fields. In the situation where the free energy

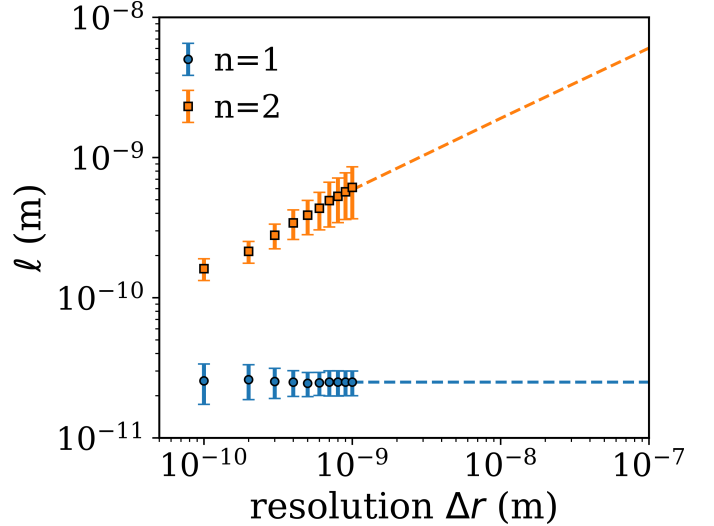


Figure 9: Internal length averaged over all misorientation angles, as a function of spatial resolution, for [001] symmetrical tilt grain boundaries in copper. Standard deviation is also indicated. The dotted lines show the trend for larger resolutions, using equation (20).

functional involves the Nye dislocation density tensor, Jebahi et al. [12] investigated the influence of energy functional form and internal length on material's hardening and yield strength. By fitting an energetic characteristic length scale based on a general non-quadratic power-law form with an adjusted power exponent  $n$ , their study reveals that the internal length is an intrinsic parameter of the material and should be of the order of micrometers. At a finer scale, continuum modeling based on the mechanical theory of dislocation fields relate size effects in channel-type microstructures, whereby the relevant internal length is the order of the channel width [41]. At the atomic scale, Po et al. [42] introduced a characteristic length scale parameter in a gradient elasticity formulation to accurately represent the near-core stresses generated by dislocations [42]. Their findings for various dislocations indicate that there is no single characteristic internal length, and that the length scale is significantly dependent on the type of dislocation. Importantly, they demonstrated that the internal length scale is on the order of the interatomic distances, as in our present study of grain boundary core structures and energies. From these findings, it clearly appears that the magnitude of  $\ell$  in strain gradient models should vary significantly depending on the specific mechanisms or defects modeled, spanning from the angstrom scale, to the micrometer scale.

In the present work focused on the core structure and energy of GB, our assessment of the optimized internal length value, using a quadratic ( $n = 2$ ) defect energy formulation, revealed that  $\ell$  is on the order of a few angstroms. We can further correlate its value with the atomic structural defects (structural units) composing the different GB, thereby providing a physical interpretation of this characteristic length parameter. In agreement with Po et al. [42], we also find that  $\ell$  is not a constant but depends on the defects studied. A dependence of the internal length scale on the type of GB was also suggested by using a

strain gradient plasticity model [40]. Our results for  $n = 1$  also indicate that  $\ell$  is small and depends on the defects modeled, although the relation to the atomic structure of GBs is less evident. At the atomic scale, we thus think that the power exponent  $n = 2$  is more appropriate than  $n = 1$ . As we model structural units by equivalent local dislocation densities and the energy of dislocations is proportional to the squared Burgers vector, the value  $n = 2$  seems again to be more appropriate. This is however in contradiction with Read and Shockley based models of GB energies, such as the model by Van Beers et al. [31], which rather suggest a power exponent  $n = 1$ . In such models however, the GBs are seen at some upper spatial resolution scale, and they are described by a uniform interfacial dislocation density, which basically accommodates the GB misorientation. As such, these interfacial dislocation densities can be regarded as GB curvature, which is typically what is observed in EBSD at the micron scale. In this situation, our results for the largest spatial resolutions tested, where elastic strains are missed and the GBs are seen as elastic curvatures, also suggest that a power exponent  $n = 1$  should be more appropriate. Our choice is motivated by the fact that  $\ell$  does not depend on spatial resolution for  $n = 1$ , as should be, while it does for  $n = 2$ .

These analyses thus imply the need for a careful consideration of spatial resolution effects, i.e., the scale at which we look at GBs, when interpreting and calibrating strain gradient based free energy functionals. In the present study, it appears that  $n = 2$  is more appropriate when explicitly resolving each defect composing GBs, while  $n = 1$  is a better choice for modeling GBs as curvatures at higher scales. However, if one decides to keep a power exponent  $n = 2$  even for larger spatial resolutions, then the internal length increases with spatial resolution, and its value for resolutions the order of the micron becomes closer to values typically considered in strain gradient plasticity modeling of GBs [12].

## 8. Conclusions

In summary, our study has introduced a methodology that merges atomistic simulations with continuum mechanics to explore the utilization of defects energy functional, employing the dislocation density tensor within strain gradient plasticity models. This approach has demonstrated considerable success in predicting grain boundary energies across various misorientations in copper. At its core, we employed an atomistic-to-continuum framework that describes the atomistic structure of grain boundary cores through an equivalent continuous Nye dislocation density tensor field. This framework relied on fast Fourier transform field dislocation mechanics simulations incorporating atomistically informed input dislocation density. One key advantage of this methodology is its capacity to predict the elastic fields linked with defect distribution within all grain boundaries types, ranging from low-angle grain boundaries with isolated dislocations to high-angle grain boundaries with complex structural units.

Our approach accurately capture the physics of the energy of high-angle grain boundaries, as it reveals cusps in elastic

strain energy. These cusps arise from the remarkable proximity of neighboring structural unit, leading to a self-screening effect on the elastic fields. By partitioning the total energy of a grain boundaries acquired through molecular static simulations, in the same way as in the Read-Schokley model, we have predicted the core energy of GBs adjusting the energetic length scale within a generalized defect energy formulation inspired by the Gurtin-type strain gradient crystal plasticity framework. Particularly noteworthy is the significant correlation between the internal length scale and the topology of structural units composing grain boundaries, particularly pronounced when  $n = 2$  and at lower FFT grid resolutions. More precisely, the internal length scale origin from the type and sequence of these atomistic structural units.

We emphasize the critical impact of FFT grid resolution on the internal length scale, with distinct behaviors observed at different resolutions. At higher resolutions, the internal length scale's relationship with grain boundary misorientation angle takes on distinct shapes. Notably, our findings also indicate the independence of the internal length scale from FFT resolution in the case of  $n = 1$ . Hence, it appears that  $n = 2$  is more appropriate when explicitly resolving each defect composing GBs, while  $n = 1$  is a better choice for modeling GBs as curvatures at higher scales.

## CRedit authorship contribution statement

**Houssam Kharouji:** Data curation, Formal analysis, Investigation, Methodology, Visualization, Writing – original draft, Writing – review & editing. **Vincent Taupin:** Conceptualization, Formal analysis, Investigation, Methodology, Supervision, Validation, Writing – review & editing. **Julien Guéno**lé: Conceptualization, Funding acquisition, Investigation, Project administration, Resources, Supervision, Writing – review & editing.

## Declaration of competing interest

The authors declare that they have no known competing financial interests or personal relationships that could have appeared to influence the work reported in this paper.

## Acknowledgments

The authors wish to thank Dr. Mohamed Jebahi (LEM3, Arts et Métiers) for fruitful discussions, and acknowledge funding from the LabEx DAMAS (Laboratory of Excellence on Design of Alloy Metals for low-mAss Structures). H.K acknowledges financial support from the Région Grand-Est. V.T. and J.G. acknowledge funding from the French National Research Agency (ANR), Grant ANR-21-CE08-0001 (ATOUM). High Performance Computing resources were provided by the EXPLOR center of the Université de Lorraine and by GENCI at TGCC (Grant 2022-A0120911390, 2023-AD010911390R1 and 2023-A0150914654).

## References

- [1] E. O. Hall, The deformation and ageing of mild steel: Iii discussion of results, *Proceedings of the Physical Society. Section B* 64 (9) (1951) 747–753. doi:10.1088/0370-1301/64/9/303.
- [2] N. J. Petch, The cleavage strength of polycrystals, *Journal of the Iron and Steel Institute* 174 (1953) 25–28.
- [3] M. Ghorbani Moghaddam, A. Achuthan, B. A. Bednarczyk, S. M. Arnold, E. J. Pineda, Grain size-dependent crystal plasticity constitutive model for polycrystal materials, *Materials Science and Engineering: A* 703 (2017) 521–532. doi:10.1016/j.msea.2017.07.087.
- [4] H. Askes, E. C. Aifantis, Gradient elasticity in statics and dynamics: An overview of formulations, length scale identification procedures, finite element implementations and new results, *International Journal of Solids and Structures* 48 (13) (2011) 1962–1990. doi:10.1016/j.ijsolstr.2011.03.006.
- [5] N. Fleck, G. Muller, M. Ashby, J. Hutchinson, Strain gradient plasticity: Theory and experiment, *Acta Metallurgica et Materialia* 42 (2) (1994) 475–487. doi:10.1016/0956-7151(94)90502-9.
- [6] E. C. Aifantis, On the microstructural origin of certain inelastic models, *Journal of Engineering Materials and Technology* 106 (4) (1984) 326–330. doi:10.1115/1.3225725.
- [7] E. C. Aifantis, The physics of plastic deformation, *International Journal of Plasticity* 3 (3) (1987) 211–247. doi:10.1016/0749-6419(87)90021-0.
- [8] M. F. Ashby, The deformation of plastically non-homogeneous materials, *The Philosophical Magazine: A Journal of Theoretical Experimental and Applied Physics* 21 (170) (1970) 399–424. doi:10.1080/14786437008238426.
- [9] A. Acharya, Lattice incompatibility and a gradient theory of crystal plasticity, *Journal of the Mechanics and Physics of Solids* 48 (8) (2000) 1565–1595. doi:10.1016/s0022-5096(99)00075-7.
- [10] M. E. Gurtin, L. Anand, Thermodynamics applied to gradient theories involving the accumulated plastic strain: The theories of aifantis and fleck and hutchinson and their generalization, *Journal of the Mechanics and Physics of Solids* 57 (3) (2009) 405–421. doi:10.1016/j.jmps.2008.12.002.
- [11] S. Forest, N. Guéinichault, Inspection of free energy functions in gradient crystal plasticity, *Acta Mechanica Sinica* 29 (6) (2013) 763–772. doi:10.1007/s10409-013-0088-0.
- [12] M. Jebahi, L. Cai, F. Abed-Meraim, Strain gradient crystal plasticity model based on generalized non-quadratic defect energy and uncoupled dissipation, *International Journal of Plasticity* 126 (2020) 102617. doi:10.1016/j.ijplas.2019.10.005.
- [13] S. Wulfinghoff, S. Forest, T. Böhlke, Strain gradient plasticity modeling of the cyclic behavior of laminate microstructures, *Journal of the Mechanics and Physics of Solids* 79 (2015) 1–20. doi:10.1016/j.jmps.2015.02.008.
- [14] M. E. Gurtin, A gradient theory of single-crystal viscoplasticity that accounts for geometrically necessary dislocations, *Journal of the Mechanics and Physics of Solids* 50 (1) (2002) 5–32. doi:10.1016/s0022-5096(01)00104-1.
- [15] A. Panteghini, L. Bardella, On the finite element implementation of higher-order gradient plasticity, with focus on theories based on plastic distortion incompatibility, *Computer Methods in Applied Mechanics and Engineering* 310 (2016) 840–865. doi:10.1016/j.cma.2016.07.045.
- [16] M. GURTIN, A gradient theory of small-deformation isotropic plasticity that accounts for the burgers vector and for dissipation due to plastic spin, *Journal of the Mechanics and Physics of Solids* 52 (11) (2004) 2545–2568. doi:10.1016/j.jmps.2004.04.010.
- [17] I. Groma, F. Csikor, M. Zaiser, Spatial correlations and higher-order gradient terms in a continuum description of dislocation dynamics, *Acta Materialia* 51 (5) (2003) 1271–1281. doi:10.1016/s1359-6454(02)00517-7.
- [18] W. T. Read, W. Shockley, Dislocation models of crystal grain boundaries, *Physical Review* 78 (3) (1950) 275–289. doi:10.1103/physrev.78.275.
- [19] H. Kharouji, L. Dezerald, P. Hirel, P. Carrez, P. Cordier, V. Taupin, J. Guérolé, Atomistic to continuum mechanics description of crystal defects with dislocation density fields: Application to dislocations and grain boundaries, *International Journal of Plasticity* 177 (2024) 103990. doi:10.1016/j.ijplas.2024.103990.
- [20] A. P. Thompson, H. M. Aktulga, R. Berger, D. S. Bolintineanu, W. M. Brown, P. S. Crozier, P. J. in 't Veld, A. Kohlmeyer, S. G. Moore, T. D. Nguyen, R. Shan, M. J. Stevens, J. Tranchida, C. Trott, S. J. Plimpton, Lamm - a flexible simulation tool for particle-based modeling at the atomic, meso, and continuum scales, *Computer Physics Communications* 271 (2022) 108171. doi:10.1016/j.cpc.2021.108171.
- [21] Y. Mishin, M. J. Mehl, D. A. Papaconstantopoulos, A. F. Voter, J. D. Kress, Structural stability and lattice defects in copper: ab initio, tight-binding, and embedded-atom calculations, *Physical Review B* 63 (22) (2001). doi:10.1103/physrevb.63.224106.
- [22] M. A. Tschopp, S. P. Coleman, D. L. McDowell, Symmetric and asymmetric tilt grain boundary structure and energy in cu and al (and transferability to other fcc metals), *Integrating Materials and Manufacturing Innovation* 4 (1) (2015) 176–189. doi:10.1186/s40192-015-0040-1.
- [23] H. D., B. D.J., *Introduction to Dislocations*, Elsevier, 2011. doi:10.1016/c2009-0-64358-0.
- [24] E. Kröner, Incompatibility, defects, and stress functions in the mechanics of generalized continua, *International Journal of Solids and Structures* 21 (7) (1985) 747–756. doi:10.1016/0020-7683(85)90077-0.
- [25] A. Acharya, A model of crystal plasticity based on the theory of continuously distributed dislocations, *Journal of the Mechanics and Physics of Solids* 49 (4) (2001) 761–784. doi:10.1016/s0022-5096(00)00060-0.
- [26] S. Berbenni, V. Taupin, K. S. Djaka, C. Fressengeas, A numerical spectral approach for solving elasto-static field dislocation and g-disclination mechanics, *International Journal of Solids and Structures* 51 (23–24) (2014) 4157–4175. doi:10.1016/j.ijsolstr.2014.08.009.
- [27] K. S. Djaka, A. Villani, V. Taupin, L. Capolungo, S. Berbenni, Field dislocation mechanics for heterogeneous elastic materials: A numerical spectral approach, *Computer Methods in Applied Mechanics and Engineering* 315 (2017) 921–942. doi:10.1016/j.cma.2016.11.036.
- [28] C. HARTLEY, Y. MISHIN, Characterization and visualization of the lattice misfit associated with dislocation cores, *Acta Materialia* 53 (5) (2005) 1313–1321. doi:10.1016/j.actamat.2004.11.027.
- [29] C. S. Hartley, Y. Mishin, Representation of dislocation cores using nye tensor distributions, *Materials Science and Engineering: A* 400–401 (2005) 18–21. doi:10.1016/j.msea.2005.03.076.
- [30] H. Grimmer, A reciprocity relation between the coincidence site lattice and the dsc lattice, *Scripta Metallurgica* 8 (11) (1974) 1221–1223. doi:10.1016/0036-9748(74)90334-2.
- [31] P. van Beers, V. Kouznetsova, M. Geers, M. Tschopp, D. McDowell, A multiscale model of grain boundary structure and energy: From atomistics to a continuum description, *Acta Materialia* 82 (2015) 513–529. doi:10.1016/j.actamat.2014.08.045.
- [32] L. Priester, *Grain Boundaries: From Theory to Engineering*, Springer Netherlands, 2013. doi:10.1007/978-94-007-4969-6.
- [33] A. Stukowski, Visualization and analysis of atomistic simulation data with ovito—the open visualization tool, *Modelling and Simulation in Materials Science and Engineering* 18 (1) (2009) 015012. doi:10.1088/0965-0393/18/1/015012.
- [34] A. P. Sutton, V. Vitek, On the structure of tilt grain boundaries in cubic metals i. symmetrical tilt boundaries, *Philosophical Transactions of the Royal Society of London. Series A, Mathematical and Physical Sciences* 309 (1506) (1983) 1–36. doi:10.1098/rsta.1983.0020.
- [35] G. Bishop, B. Chalmers, A coincidence — ledge — dislocation description of grain boundaries, *Scripta Metallurgica* 2 (2) (1968) 133–139. doi:10.1016/0036-9748(68)90085-9. URL [http://dx.doi.org/10.1016/0036-9748\(68\)90085-9](http://dx.doi.org/10.1016/0036-9748(68)90085-9)
- [36] J. W. Cahn, Y. Mishin, A. Suzuki, Coupling grain boundary motion to shear deformation, *Acta Materialia* 54 (19) (2006) 4953–4975. doi:10.1016/j.actamat.2006.08.004. URL <http://dx.doi.org/10.1016/j.actamat.2006.08.004>
- [37] W. Gui-Jin, V. Vitek, Relationships between grain boundary structure and energy, *Acta Metallurgica* 34 (5) (1986) 951–960. doi:10.1016/0001-6160(86)90068-4.
- [38] D. Wolf, Structure-energy correlation for grain boundaries in f.c.c. metals—i. boundaries on the (111) and (100) planes, *Acta Metallurgica* 37 (7) (1989) 1983–1993. doi:10.1016/0001-6160(89)90082-5.
- [39] C. Fressengeas, V. Taupin, L. Capolungo, Continuous modeling of the structure of symmetric tilt boundaries, *International Journal of Solids and Structures* 51 (6) (2014) 1434–1441. doi:10.1016/j.ijsolstr.2013.12.031.
- [40] E. Bayerschen, M. Stricker, S. Wulfinghoff, D. Weygand, T. Böhlke, Equivalent plastic strain gradient plasticity with grain boundary hardening and comparison to discrete dislocation dynamics, *Proceedings of the Royal Society A: Mathematical, Physical and Engineering Sciences*

471 (2184) (2015) 20150388. doi:10.1098/rspa.2015.0388.

- [41] V. Taupin, S. Berbenni, C. Fressengeas, Size effects on the hardening of channel-type microstructures: A field dislocation mechanics-based approach, *Acta Materialia* 60 (2) (2012) 664–673. doi:10.1016/j.actamat.2011.10.033.
- [42] D. Seif, G. Po, M. Mrovec, M. Lazar, C. Elsässer, P. Gumbsch, Atomistically enabled nonsingular anisotropic elastic representation of near-core dislocation stress fields in  $\alpha$ -iron, *Physical Review B* 91 (18) (May 2015). doi:10.1103/physrevb.91.184102.